New Structural Motif in Hexagonally Ordered Cylindrical Ternary (ABC) Block Copolymer Microdomains

Susanne Brinkmann,[†] Reimund Stadler,[‡] and Edwin L. Thomas*[,§]

Institut für Organische Chemie, J. J. Becherweg 18−20, 55099 Mainz, Germany, Makromolekulare Chemie II, Universität Bayreuth, 95440 Bayreuth, Germany, and Department of Materials Science and Engineering, Massachusetts Institute of Technology, 77 Massachusetts Avenue, Cambridge, Massachusetts 02139

Received January 26, 1998; Revised Manuscript Received June 26, 1998

ABSTRACT: The morphologies of a polystyrene-*block*-polybutadiene-*block*-poly(methyl methacrylate) triblock copolymer (SBM) with polybutadiene as the majority component as they are cast from different solvents and solvent mixtures are determined using transmission electron microscopy (TEM) and small-angle X-ray scattering (SAXS) techniques. Besides a lamellar morphology and microphase separated structures of poor long-range order, a morphology is identified in which both A (polystyrene, PS) and C (poly(methyl methacrylate), PMMA) chains form separate cylindrical microdomains. In contrast to the square (*p*4*mm*) symmetry for the cylinder arrangement which has been discussed in the case of ABC triblock copolymers with B being the matrix forming component, we now report the formation of a new morphological motif of hexagonal (*p*6*mm*) symmetry, where A and C form two kinds of cylindrical microdomains in a B matrix.

Introduction

During the past decades the periodic morphologies of AB diblock and ABA triblock copolymers consisting of two chemically different components have been studied in detail.[1,2] The influence of the incompatibility, as well as the influence of the composition and degree of polymerization, on the formation of the morphology is quite well understood.[3,4] Morphological studies of ternary ABC triblock copolymers consisting of three chemically different segments have been of more recent interest, both in experimental[5−7] and theoretical studies.[8,9] In the case of cylindrical morphologies two classes of morphologies can be discussed. On one hand one of the end blocks can be the matrix forming component.[10,11] On the other hand the center block B can be the matrix forming component, and A and C form cylindrical microdomains. In such polymers the cylinders have been reported not to arrange hexagonally but rather on a square lattice.[12−14]

The theoretical investigations[8,9] demonstrate that a square lattice packing of cylinders formed by two immiscible end blocks in the matrix of the center block is favored in comparison to a "pseudohexagonal" packing. Theoretical packing patterns that have been discussed in the literature are shown in Figure 1a,b. Analysis of the symmetry elements of the pattern shown in Figure 1b shows that it does not correspond to a hexagonal packing with *p6mm* symmetry but is a rectangular lattice (cell parameters *a* and *b*) with *p*2*mm* symmetry. The symmetry of the cylinder packing is now pseudohexagonal with $a = \sqrt{3}b$. As a result of this cylinder packing, each block has to distort anisotropically in space.[8] Comparing the free energies of these two systems for symmetric (i.e. $\phi_A = \phi_C$) ABC triblock copolymers, the theoretical calculations showed that for $\phi_A = \phi_C < 0.36$ cylinders on a square lattice

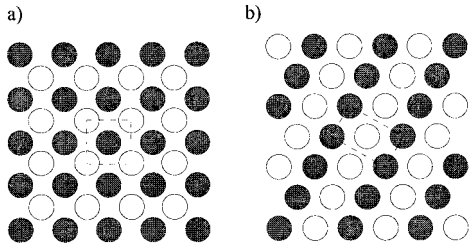

Figure 1. Packing patterns as stated by Mogi et al.: (a) square packing; (b) hexagonal packing.[14]

are thermodynamically more favorable than cylinders that are pseudohexagonally packed.[8] The authors denote that square arrayed cylinders become more stable than ABCBA lamellae at $\phi_A = \phi_C = 0.230$. Polymers with volume fractions smaller than $\phi_A = \phi_C = 0.14$ are expected to form spherical microdomains that are arranged on a CsCl-type structure (space group $Pm\bar{3}m$).[8]

In addition to the cylindrical morphologies described so far, morphologies combining lamellar and cylindrical motifs have been reported. Auschra et al. observed cylindrical microdomains of the minority center block component (polybutadiene (PB)) along the polystyrene/poly(methyl methacrylate) (PS/PMMA) lamellar interface in a polystyrene-*block*-polybutadiene-*block*-poly(methyl methacrylate) (SBM) triblock copolymer.[6,15] This microdomain geometry has also been confirmed by the theoretical calculations of Zheng and Wang.[9] They also predict the existence of a morphology where the minority species A (one of the end blocks) forms cylindrical domains located regularly inside the B domains of a B/C lamellar stacking for ABC triblock copolymers. Such a morphology has been observed in polybutadiene-*block*-polystyrene-*block*-poly(methyl methacrylate) block copolymers.[16] In this contribution we report the formation of a new cylindrical morphology with hexagonal symmetry which has neither been observed nor previously predicted. The dependence of the morphology on the casting solvent will also be discussed.

[†] Institut für Organische Chemie.
[‡] Universität Bayreuth.
[§] Massachusetts Institute of Technology.

S0024-9297(98)00103-X CCC: $15.00
Published on Web 08/25/1998

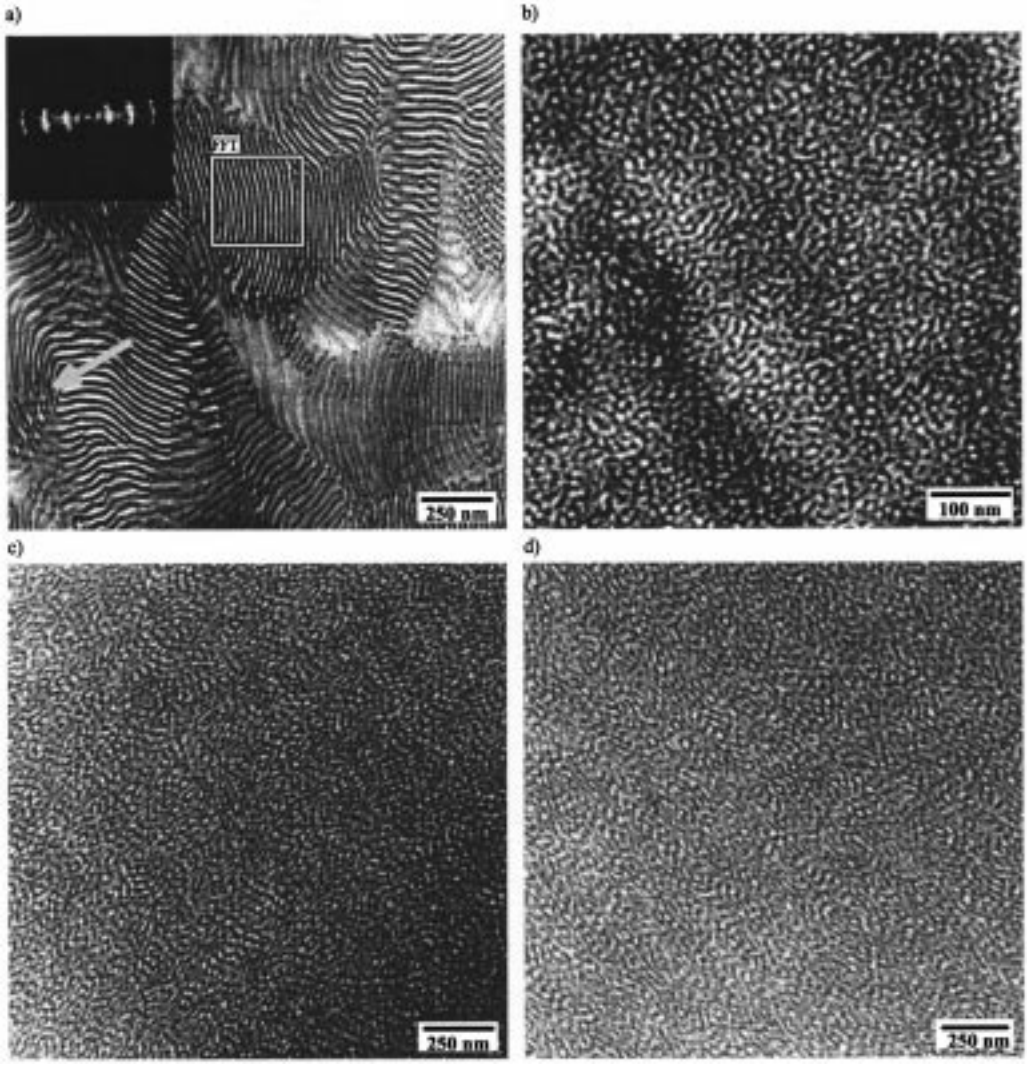

Figure 2. TEM micrographs of solvent cast films of $S_{23}B_{57}M_{20}^{215}$ in various casting solvents: (a) chloroform; (b) toluene; (c) benzene/cyclohexane (50:50); (d) benzene/cyclohexane (70:30).

Experimental Section

Synthesis and Characterization. The synthesis of the SBM triblock copolymer was carried out via sequential anionic polymerization in tetrahydrofuran (THF) in the presence of lithium alkoxides using *sec*-butyllithium as initiator. Details of the polymerization procedure have been described previously.[17] The composition of the block copolymer was determined using ^{1}H NMR spectroscopy. The molecular weight was calculated using results from size exclusion chromatography (GPC) of the styrene precursor polymer in combination with ^{1}H NMR spectroscopy. It has been shown previously that this method results in molecular weights comparable with those obtained by osmometry.[17] GPC analysis was performed on a Waters GPC equipped with polystyrene gel columns with porosities of 10^5, 10^4, 10^3, and 10^2 Å, using UV and RI detectors and THF as solvent. The copolymer is described as $S_{23}B_{57}M_{20}^{215}$ where 23, 57, and 20 correspond to the weight percentage of the components with a total number average molecular mass of 215 kg/mol. The polydispersity of the triblock copolymer is $M_w/M_n = 1.03$. The polybutadiene block is predominantely (90%) formed by 1,2-units.

Transmission Electron Microscopy. Transparent films were cast from 5% (w/v) solutions using chloroform, toluene, and mixtures of benzene and cyclohexane (30:70, 50:50, 70:30) as solvents. The solvent was slowly evaporated over a period of 3 weeks. The films were subsequently dried in vacuo for 2 days before annealing at 120 °C for 3−5 days. Ultrathin sections of the as-cast films were obtained using a Reichert ultramicrotome (FC4 cryo attachment) equipped with a diamond knife. Because the sample was not rigid enough at room temperature, the cutting was performed at −120 °C under cryo conditions. The ultrathin sections were stained by exposing them for 2 h to the vapor over an OsO_4 solution (10% in water). Transmission electron microscopy (TEM) was performed in the bright field mode on a JEOL 200 CX microscope operating at 200 kV.

Small-Angle X-ray Scattering. The small-angle X-ray scattering experiments were performed at the time-resolved diffraction facility (station X12B) of the National Synchrotron Light Source at Brookhaven National Laboratory (BNL).

Results and Discussion

Parts a−d of Figure 2 show the TEM micrographs of solvent cast films of $S_{23}B_{57}M_{20}^{215}$. In films cast from chloroform solution a lamellar morphology is observed (Figure 2a). The PB phase is stained by the OsO_4 vapor and appears dark. PMMA and PS are unstained and appear light. The long period which can be obtained from TEM micrographs is 41 nm (ABCBA repeat distance). The lamellar structure is confirmed by SAXS experiments, as shown in Figure 3a. Although the first-order peak of the SAXS pattern is hidden by the beam stop, the characteristic reflections ((200), (300), (400), (600), (800)) are observed. By plotting d_{n00} versus the reciprocal of the scattering order, the d spacing of the

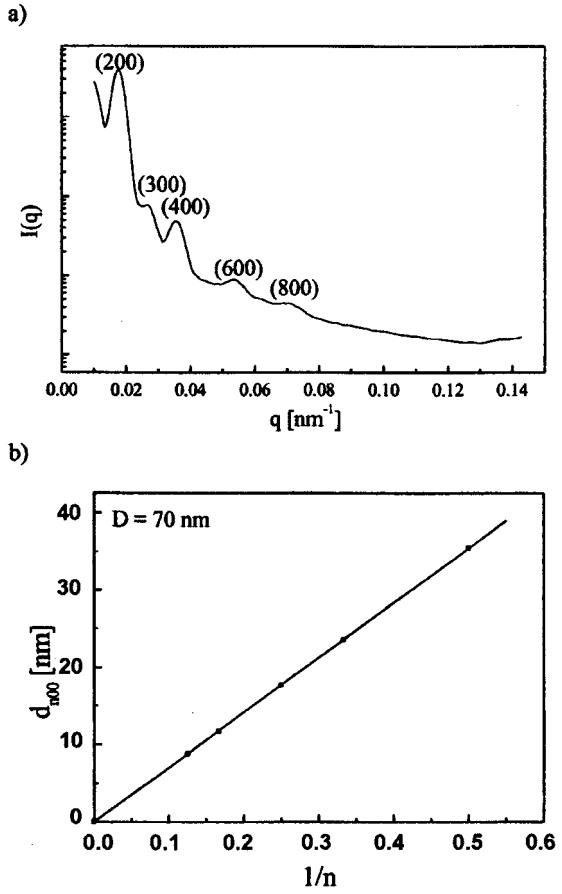

Figure 3. (a) Small-angle X-ray pattern of $S_{23}B_{57}M_{20}^{215}$ cast from chloroform; (b) d_{n00} as a function of the reciprocal scattering order.

lamellar long period can be determined from the slope (Figure 3b). For $S_{23}B_{57}M_{20}^{215}$ the long period is 71 nm. The large difference between SAXS and TEM long periods in the case of PMMA containing block copolymers has been observed before.[18,19] From the TEM micrograph it can be clearly seen that the sample is not very well ordered. The grains are relatively small. The arrow in Figure 2a indicates an area close to a grain boundary, where the lamellae rupture to form cylindrical microdomains. These areas, however, are relatively small and can only be observed in some places close to the grain boundaries. This already indicates that this lamellar morphology might not correspond to the thermodynamic equilibrium. In comparison to other SBM triblock copolymers exhibiting a lamellar morphology, but with lower B volume fraction ($\phi_B \approx 0.35$) for which the long period has been shown to be given by[18,19]

$$D = 0.063M_n^{0.619} \quad (1)$$

the long period of the present lamellar morphology is considerably smaller (70 nm versus 125 nm according to eq 1). It is unlikely that this large difference may be attributed to the higher polybutadiene fraction but rather to the nonequilibrium nature of this structure: Chloroform is a relatively bad solvent for polybutadiene. Thus the majority component tends to segregate first. When the structure is frozen, the more swollen PS and PMMA chains occupy volume fractions which are larger than that corresponding to the bulk composition and give rise to the nonequilibrium lamellar assembly upon drying.

A second sample was prepared from toluene solution. The corresponding TEM micrograph is shown in Figure 2b. This sample is still microphase separated but does not show any long-range order at all; rather the structure exhibits small-scale fluctuations. Unannealed samples and samples that had been annealed for 3 h or 5 days respectively at 120 °C showed the same morphology. Toluene is a good solvent for all components. The high molecular weight of the sample apparently prohibits the formation of a long-range ordered microdomain structure during toluene evaporation. From the experience gathered in handling other ternary block copolymers a more promising appoach to equilibrium morphology is to use a relatively bad solvent for the minority component(s).

To further evaluate the influence of the casting solvent quality on the morphology, films were thus cast from solvent mixtures. Benzene and cylcohexane were chosen as solvents because benzene like toluene is a good solvent for all three block copolymer components, whereas cyclohexane is a nonsolvent for PMMA and a Θ-solvent for PS. Furthermore, the vapor pressures of the two solvents are comparable (benzene, 100 mmHg at 26.1 °C; cyclohexane, 100 mmHg at 25.5 °C),[20] which should result in an approximately constant solvent composition during evaporation. By changing the ratio of cyclohexane to benzene, the quality of the solvent with regard to the PMMA and PS end blocks can be conveniently varied. For samples cast from solvent mixtures with $\phi_{cyclohexane} < 50\%$, the same morphology is observed as in the case of films cast from toluene (Figure 2c,d). When cast from a benzene:cyclohexane (30:70) mixture, a morphology consisting of hexagonally packed cylinders is formed (Figure 4a).

There are two types of cylindrical microdomains in the PB matrix distinguished by their respective diameters rather than their bright field contrast. The diameters obtained from TEM of the different cylinders are 14 ± 2 and 18 ± 2 nm. Each Z_α cylinder is surrounded by six Z_ω cylinders and each Z_ω cylinder by three Z_α cylinders, yielding a ratio of two thin cylinders (Z_ω) per one thick cylinder (Z_α). Figure 4b shows the SAXS pattern for this sample. The first two maxima are located at **q** vectors 1:1.72 in agreement with a hexagonal cylindrical arrangement. These scattering maxima thus should be attributed to the (100) and (110) reflections. At larger **q** values (around 0.5 nm^{-1}) a broad maximum is observed which might be attributed to the cylinder form factor. In usual hexagonal block copolymer lattices the (100) reflection always has the highest intensity. We discuss this feature later. The structure that we propose, displays a hexagonal symmetry with respect to each cylinder type (Figure 5). This hexagonal coarray of cylinders has not been reported or predicted before. Figure 5a shows the arrangement of Z_α cylinders. It is identical to the hexagonal array of cylinders observed in AB or ABA block copolymers and belongs to the *p*6*mm* plane group.

The thin cylinders Z_ω arrange also on a hexagonal lattice where the center cylinder is missing (Figure 5b). The structure resulting from the addition of Figure 5a,b is shown in Figure 5c. Analysis of the unit cell and symmetry elements shows that structure is hexagonal with *p*6*mm* symmetry in the case of Figures 5b,c, though the motif differs from a simple hexagonal packing. The unit cells of the different hexagonal lattices including the symmetry elements are also given.

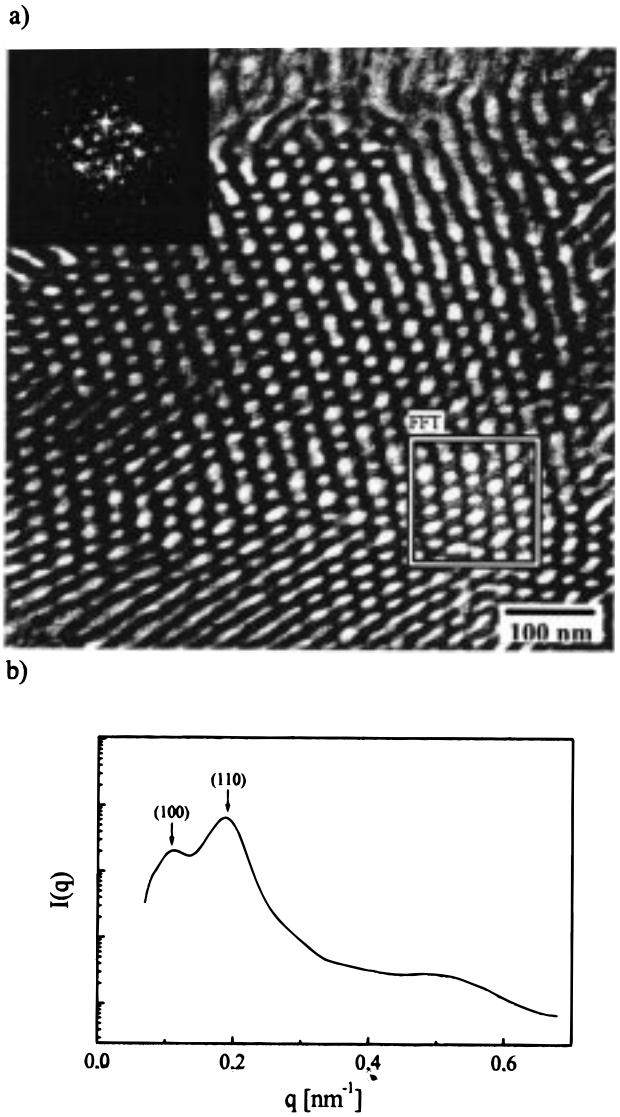

Figure 4. $S_{23}B_{57}M_{20}^{215}$ cast from benzene/cyclohexane (30:70): (a) TEM micrograph; (b) SAXS pattern.

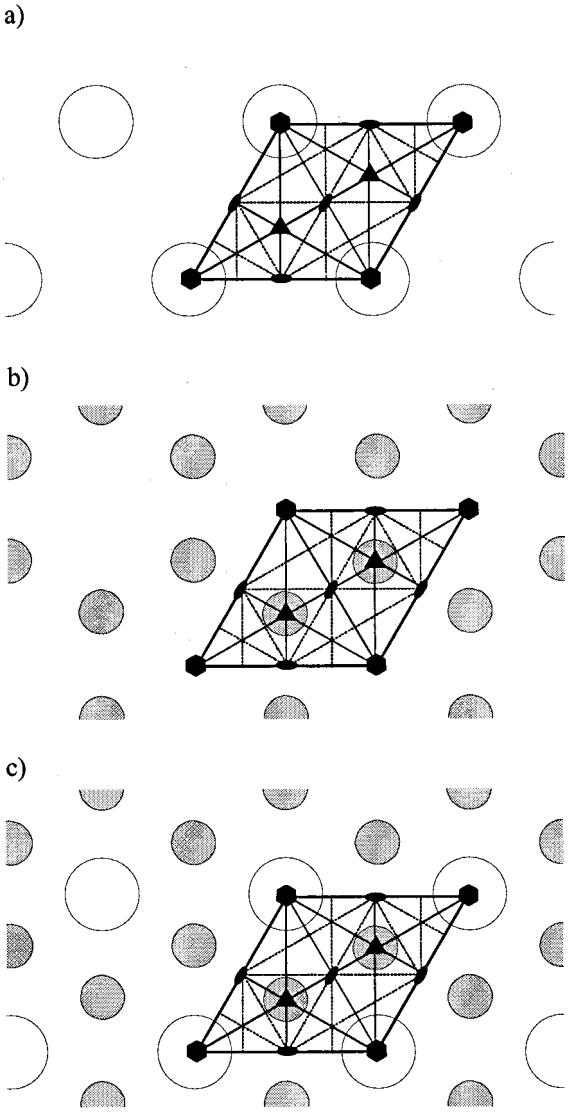

Figure 5. Unit cells and symmetry elements of the different lattices: (a) Z_α cylinders; (b) Z_ω cylinders; (c) combination of structures a and b.

It is evident that two thin cylinders Z_ω and one thick cylinder Z_α are present per unit cell.

Before attempting an assignment of the Z_α and Z_ω cylinders to polystyrene or poly(methyl methacrylate), respectively, the consequences of the different *p*6*m* motifs (Figure 5a−c) to the scattering will be discussed.

Figure 6a−c shows a larger area of the real space motifs and the corresponding Fourier transforms (FT) (Figure 6d−f). The assignment of the FT of Figure 6f is given in Figure 7a. For the assignment of the FT the *hkl* indexing was used where the magnitude of the scattering vector is given by $(h^2 + hk + k^2)^{1/2}$.

The hexagonal symmetry can easily be verified in all cases. The most striking difference is observed in the relative intensities of the (100) (≡(010)) and (110) (≡(1$\bar{1}$0)) reflections. While (100) has the highest intensity in a "conventional" hexagonal arrangement (Figure 6e), the intensity of the (100) reflection is weaker than the intensity of the (110) reflection for the new motif. Figures 7b shows a larger magnification of the FT of $S_{23}B_{57}M_{20}^{215}$. It shows approximately the same intensity distribution as the idealized lattice (Figure 6f), although the cylinders have been cut at an angle $\alpha \neq 90°$ and thus do not show a perfect end-on view. Subsequently the real image and FT are slightly distorted.

To allow direct comparison with the experimental SAXS data, the FT patterns shown in Figure 6 have been radially integrated. Two examples are given in Figure 8a,b. The intensity is plotted as a function of $\mathbf{q}/\mathbf{q}_o$, $\mathbf{q}_o$ being the scattering vector of the (100) reflection of the *p*6*mm* lattices given in Figure 6a (conventional hexagonal motif) and Figure 6c (new hexagonal motif). What has already been concluded qualitatively from the FT patterns, i.e., that the (100) reflections are lower in intensity than the (110) reflections, is now more obvious. The lower intensity of the of the (100) reflection as compared to the (110) reflections has also been observed in the experimental SAXS pattern (Figure 4b). Thus the experimental SAXS data are in good agreement with the new morphological motif derived from the TEM micrographs.

The final problem to be solved is the assignment of the thick Z_α and thin Z_ω cylinders to either one of the end blocks (PS or PMMA). The volume fractions of PS and PMMA in $S_{23}B_{57}M_{20}^{215}$ are $\phi_{PS} = 0.215$ and $\phi_{PMMA} = 0.169$. These values are calculated on the basis of

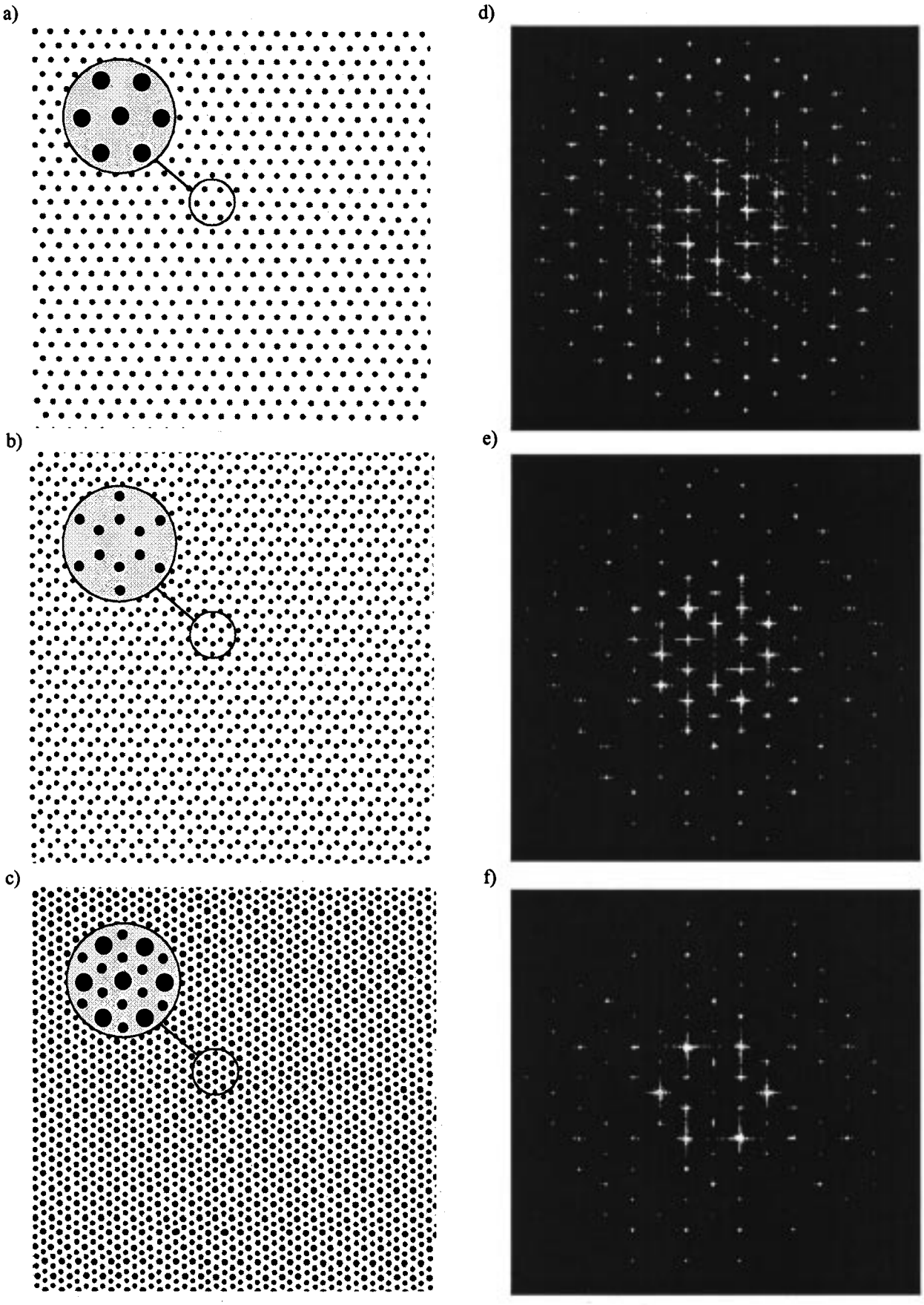

Figure 6. Real space motifs of packing patterns with *p*6*mm* symmetry for cylindrical structures and corresponding FTs: (a) hexagonal packing of Z_a; (b) hexagonal packing of Z_ω; (c) addition of structures a and b; (d) FT of structure a; (e) FT of structure b; (f) FT of structure c.

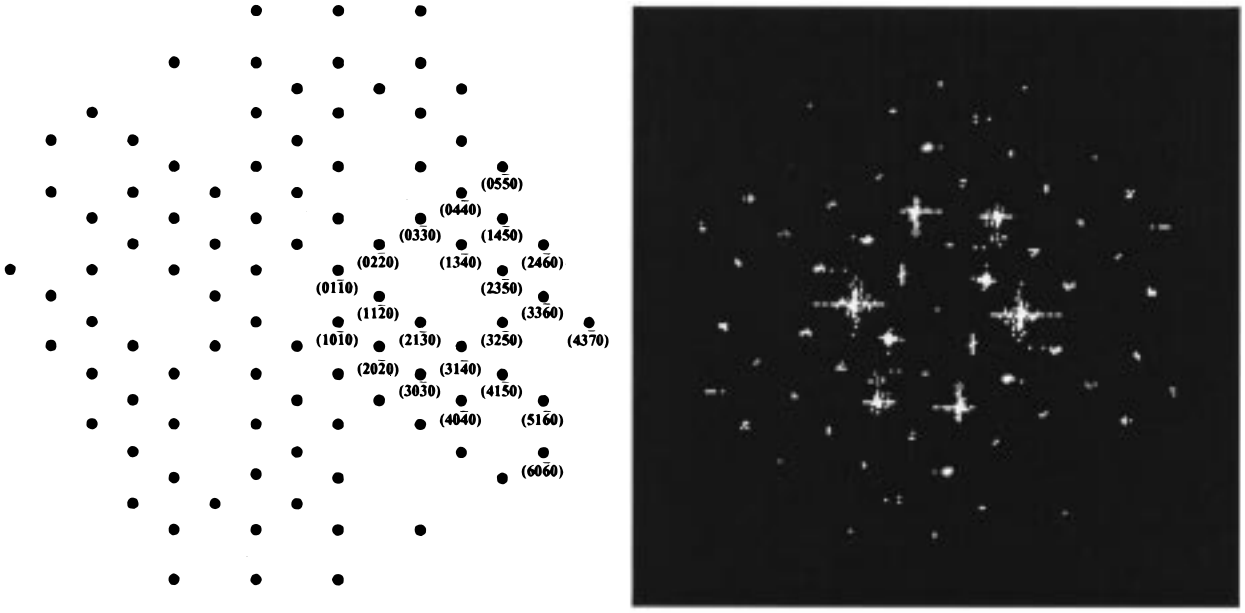

Figure 7. (a) Assignment of the FT in Figure 6f; (b) enlargement of the FT of $S_{23}B_{57}M_{20}$[215].

the weight composition under the assumption of the bulk homopolymer densities.

To assign Z_α and Z_ω, we will first calculate the cylinder diameters D_α and D_ω for the two different possibilities and compare these calculated values to the experimentally observed cylinder diameters. In a second step we will use some thermodynamic and kinetic arguments to support the cylinder assignment.

The diameters D_α and D_ω are given by

$$D_\alpha = 2\left(\frac{2}{\pi\sqrt{3}}\right)^{1/2} d\phi_\alpha{}^{1/2} \tag{2}$$

$$D_\omega = 2\left(\frac{1}{\pi\sqrt{3}}\right)^{1/2} d\phi_\omega{}^{1/2} \tag{3}$$

with d being the long spacing obtained either from SAXS or TEM.

case 1: Z_α = PMMA; Z_ω = PS

SAXS: $d = 56.6$ nm; $D_{\alpha(\mathrm{PMMA})} = 28.2$ nm; $D_{\omega(\mathrm{PS})} = 22.5$ nm; $(D_\alpha/D_\omega)^{\mathrm{SAXS}}_{\mathrm{case1}} = 1.25$

TEM: $d = 40.0$ nm; $D_{\alpha(\mathrm{PMMA})} = 19.9$ nm; $D_{\omega(\mathrm{PS})} = 15.9$ nm; $(D_\alpha/D_\omega)^{\mathrm{TEM}}_{\mathrm{case1}} = 1.25$

case 2: Z_α = PS; Z_ω = PMMA

SAXS: $d = 56.6$ nm; $D_{\alpha(\mathrm{PS})} = 31.8$ nm; $D_{\omega(\mathrm{PMMA})} = 19.9$ nm; $(D_\alpha/D_\omega)^{\mathrm{SAXS}}_{\mathrm{case2}} = 1.59$

TEM: $d = 40.0$ nm; $D_{\alpha(\mathrm{PS})} = 22.4$ nm; $D_{\omega(\mathrm{PMMA})} = 14.1$ nm; $(D_\alpha/D_\omega)^{\mathrm{TEM}}_{\mathrm{case2}} = 1.59$

The experimental cylinder diameters according to TEM are

$D_\alpha = 18 \pm 2$ nm; $D_\omega = 14 \pm 2$ nm; $(D_\alpha/D_\omega)^{\mathrm{TEM}}_{\mathrm{exptl}} = 1.28 \pm 0.3$

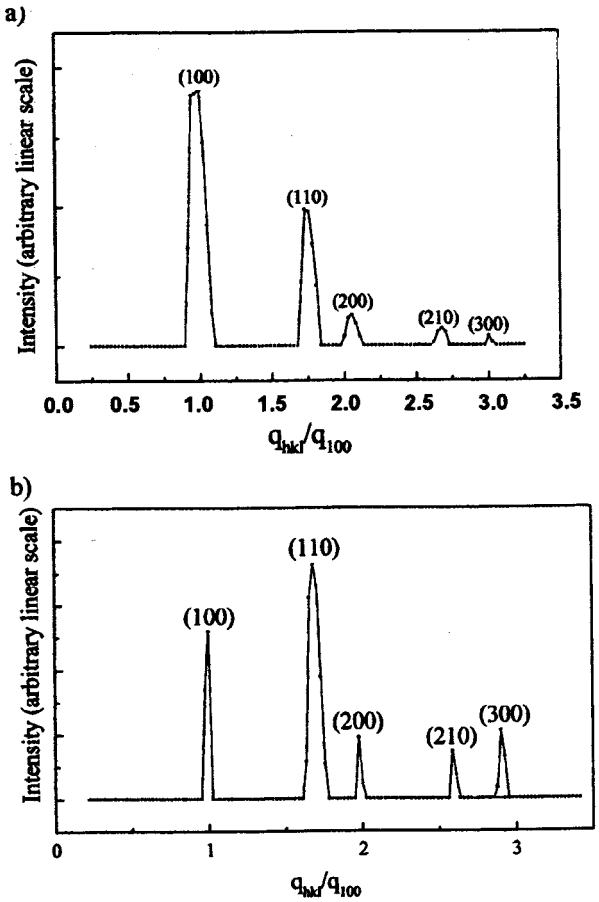

Figure 8. Radial Integration of FTs: (a) FT of hexagonal lattice (Figure 6a); (b) FT of idealized structure Figure 6c.

As in the case of the lamellar morphology described above the TEM long period is considerably smaller than the long period determined by SAXS. However as canbe seen from the ratio D_α/D_ω the experimental data (D_α = 18 nm and D_ω = 14 nm) are in closer agreement with case 1. From this we conclude that the PMMA chains form one thick Z_α cylinder and the PS chains the two thin Z_ω cylinders per unit cell.

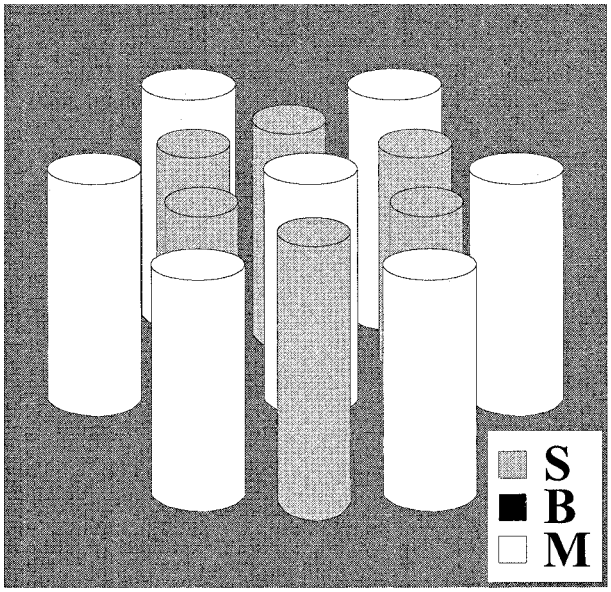

Figure 9. Schematic representation of the morphology of $S_{23}B_{57}M_{20}^{215}$.

This assignment is supported by a simple thermodynamic argument: The two relevant cohesive energy densities are $\delta_{PS/PB} = 1.1$ cal/cm^3 and $\delta_{PB/PMMA} = 1.56$ cal/cm^3.[20] The ratio of the surface energies E_α/E_ω thus can be calculated according to

$$\frac{E_\alpha}{E_\omega} = \frac{D_\alpha \delta_\alpha}{2D_\omega \delta_\omega} \tag{4}$$

Using the cylinder diameters calculated from the SAXS long period, this ratio is 0.89 for case 1 but only 0.56 for case 2. This means that the surface energies of the PS/PB and PB/PMMA intermaterial dividing surfaces (IMDS) are nearly balanced in case 1. This situation should be favored in terms of minimizing the free energy compared to a situation where the PS/PB and PB/PMMA interfacial energies areas differ by a factor of 2.

The formation of case 1 (one thick PMMA cylinder, two thin PS cylinders per unit cell) can also be rationalized by the mode of sample preparation from solution. Due to the high cyclohexane content in the solvent mixture, the PMMA block will phase segregate first during the process of solvent evaporation. The thus formed still swollen cylinders will arrange on a hexagonal lattice. In a later stage of the casting process, PS will segregate and these PS cylinders will surround the PMMA cylinders (Z_α), resulting in the hexagonal pattern for Z_ω where the center cylinders are missing.

Thus all evidence supports case 1 with a novel hexagonal motif in which the elementary cell is formed by one thick PMMA cylinder and two thinner PS cylinders (Figure 9). From the delicate thermodynamic balance which apparently is required to stabilize this structure one may conclude that the composition range where this motif is stable might be quite small. In addition this composition window should depend on the ratio in A/B and B/C incompatibility. The delicate balance is also manifested by the strong influence of the casting solvent.

Acknowledgment. The authors thank E. Prasman and B. Dair for performing the small-angle X-ray scattering experiments at Brookhaven National Laboratory. S.B. and R.S. thank Dr. D. Schollmeyer and Dr. V. Abetz for helpful discussions. Financial support from BMBF and BASF AG through Grant 03M40861 and from the *Deutsche Forschungsgemeinschaft* (DFG) through Grant SFB 262 is gratefully acknowledged. E.L.T. would like to thank the Center of Materials Science and Engineering at MIT for use of its facilities and to recognize financial support from the National Science Foundation Grant DMR 92-14853.

References and Notes

(1) Molau, G. E. *Block Copolymers*; Plenum Press: New York, 1970.
(2) Hajduk, A. D.; Harper, P. E.; Gruner, M. S.; Honeker, C. C.; Kim, G.; Thomas, E. L. *Macromolecules* **1994**, *27*, 4063−4075.
(3) Quirk, R. P.; Kinning, D. J.; Fetters, L. J. *Comprehensive Polymer Science*; Pergamon Press: Elmsford, NY, 1989; Vol. 7, p 1.
(4) Leibler, L. *Macromolecules* **1980**, *13*, 1602−1617.
(5) Stadler, R.; Auschra, C.; Beckmann, J.; Krappe, U.; Voigt-Martin, I. G.; Leibler, L. *Macromolecules* **1995**, *28*, 3080−3097.
(6) Auschra, C.; Stadler, R. *Macromolecules* **1993**, *26*, 2171−2174.
(7) Krappe, U.; Stadler, R.; Voigt-Martin, I. G. *Macromolecules* **1995**, *28*, 4558−4561.
(8) Nakazawa, H.; Ohta, T. *Macromolecules* **1993**, *26*, 5503−5511.
(9) Zheng, W.; Wang, Z.-G. *Macromolecules* **1995**, *28*, 7215−7223.
(10) Gido, S. P.; Schwark, D. W.; Thomas, E. L.; Gonçalves, M. *Macromolecules* **1993**, *26*, 2636.
(11) Breiner, U.; Krappe, U.; Abetz, V.; Stadler, R. *Macromol. Chem. Phys.* **1997**, *198*, 1051−1083.
(12) Jung, K.; Abetz, V.; Stadler, R. *Macromolecules* **1996**, *29*, 1076−1078.
(13) Mogi, Y.; Kotsuji, H.; Kaneko, Y.; Mori, K.; Matsushita, Y.; Noda, I. *Macromolecules* **1992**, *25*, 5408−5411.
(14) Mogi, Y.; Nomura, M.; Kotsuji, H.; Ohnishi, K.; Matsushita, Y.; Noda, I. *Macromolecules* **1994**, *27*, 6755−6760.
(15) Beckmann, J.; Auschra, C.; Stadler, R. *Macromol. Rapid Commun.* **1994**, *15*, 67−71.
(16) Jung, K.; Goncalves, M.; Stadler, R. Manuscript in preparation. Jung, K. Doctoral Dissertation, Mainz, Germany, 1996.
(17) Auschra, C.; Stadler, R. *Polym. Bull.* **1993**, *30*, 257−264.
(18) Breiner, U. Doctoral Dissertation, Mainz, Germany, 1996.
(19) Breiner, U.; Stadler, R.; Thomas, E. L. To be published.
(20) *CRC Handbook of Chemistry and Physics*, 55th ed.; CRC Press: Cleveland, OH, 1974.

MA980103Q